Open access • Journal Article • DOI:10.1029/2011RS004862

Estimation of the initial amplitude of plasma bubble seed perturbation from ionograms — Source link

A. J. Carrasco, A. J. Carrasco, I. S. Batista

Institutions: National Institute for Space Research, University of Los Andes

Published on: 01 Apr 2012 - Radio Science (John Wiley & Sons, Ltd)

Estimation of the initial amplitude of plasma bubble seed perturbation from ionograms

A. J. Carrasco[1,2] and I. S. Batista[2]

[1]Departamento de Física, Universidad de Los Andes (ULA), Mérida, Venezuela

[2]Instituto Nacional de Pesquisas Espaciais (INPE), São José dos Campos, Brazil

Corresponding author: Inez S. Batista
Instituto Nacional de Pesquisas Espaciais
Av. dos Astronautas, 1758, Jardim da Granja
12227-010 - São José dos Campos, SP, Brazil
Phone: +55-12-3208 7153
Fax:: +55-12-3208 6990
e-mail: inez@dae.inpe.br

Estimation of the initial amplitude of plasma bubble seed perturbation from ionograms

A. J. Carrasco[1,2] and I. S. Batista[2]

[1]Departamento de Física, Universidad de Los Andes (ULA), Mérida, Venezuela

[2]Instituto Nacional de Pesquisas Espaciais (INPE), São José dos Campos, Brazil

Abstract. This work gives the description of an experimental method for the calculation of the initial amplitude of plasma bubble seed perturbation in the bottomside F layer from ionograms. The observations show that after sunset the ionograms exhibit irregularities in the base of the F trace. In the context of the plasma depletion in the bottomside F-layer, the irregularities in ionograms can be seen like isodensity contour in evolution (in space and time). The initial amplitudes, calculated using the methodology, vary between 0.03 and 0.08. The ionograms analyzed were obtained from the station of Cachimbo (9.5° S, 54.8° W) during COPEX campaign in Brazil. The methodology can be useful for application in numerical simulation of plasma bubbles in which actual ionospheric parameters are used.

1. Introduction

Plasma instability phenomena occurring in the F-region of the equatorial ionosphere are grouped under the generic name equatorial spread F (ESF). Spread F, as exhibited by diffuse echoes on ionograms, was first reported in the first half of 20th century. After sunset, when the F-layer is lifted through the action of the ambient electric fields (from

41 F-layer dynamo), the bottomside steepens and large plasma depletions, named plasma
42 bubbles, can be generated. A number of theoretical studies and numerical simulations
43 have been made to understand the mechanism producing the plasma structures in the
44 magnetic equator. The underlying plasma physics is tied to the nonlinear evolution of
45 the generalized Rayleigh-Taylor instability (RTI) excited in the bottomside F layer. The
46 instability can be described by a situation similar to a heavy fluid resting over a light
47 fluid. The occurrence of a perturbation in the border between the fluids can lead to the
48 development of instabilities and can generate irregularities in the bottomside of the F
49 region. The evolution of these irregularities can lead to the formation of plasma bubble
50 structures. The bubble rises through the layer in response to a Rayleigh-Taylor type
51 instability. The bubble structures can extend hundreds of kilometers in altitude and in
52 both hemispheres via magnetic field lines as confirmed by many experimental
53 observations.
54
55 From October to December 2002 the Conjugate Point Equatorial Experiment (COPEX)
56 campaign was conducted in Brazil, with the objective to investigate the equatorial
57 spread *F*/plasma bubble irregularity (ESF) development conditions in terms of the
58 electrodynamical state of the ionosphere along the magnetic flux tubes in which they
59 occur. A network of instruments, including Digisondes, optical imagers, and GPS
60 receivers, was deployed at magnetic conjugate and dip equatorial locations in a
61 geometry that permitted field line mapping of the conjugate *E* layers to dip equatorial *F*
62 layer bottomside. The measurements were obtained in three localities and the ionograms
63 were taken at a 5 minutes step rate, simultaneously at the three sites. Two of these
64 localities were the magnetic conjugate points (Boa Vista, 2.8° N, 60.7° W, and Campo
65 Grande, 20.5° S, 54.7° W) and the third was located at the magnetic equator (Cachimbo,

9.5° S, 54.8° W) [*Abdu et al*., 2009a; *McNamara et al*., 2008; *Reinisch et al.*, 2004]. Using the results of the COPEX campaign, *Batista et al.* [2008] reported a velocity of rise of the order of 150 m/s for the bubbles in Cachimbo. This value corresponds to a bubble that has reached high altitude before mapping down in both hemispheres.

The observations have shown that after sunset the ionograms at the magnetic equator and low latitudes exhibit irregularities at the base of the F trace. On occasions, many discrete traces, referred in the literature as satellite traces, can be seen superposed to the main F trace, while at other times there may be no distinct structure. *Booker and Wells* [1938] interpreted these irregularities as being caused by a fast rise of F layer in the evening. The irregularities are responsible for the spread F occurrence and the rise of F layer is caused by the vertical plasma drift (pre-reversal enhancement of the zonal electric field). Several studies have suggested that the height that F layer reaches in the first hours of the night is an important parameter that controls the generation of irregularities [*Fejer et al.*, 1999]. The uplift of F layer can contribute to the destabilization of the plasma and make the instability growth rate increase with the height. Satellite traces have been frequently used as an empirical precursor of range spread F [*Abdu et al*., 1981; *Lyon et al*., 1961]. *Tsunoda* [2008], using ionogram and incoherent scatter radar data at an equatorial station, concluded that satellite traces in equatorial ionograms are direct signatures of large-scale wave structure (LSWS) which, in turns, is a more direct precursor of ESF than the post-sunset rise of the F layer.

The seeding mechanism of RTI in the development process of the plasma bubble has received special attention in recent investigations [see *Fritts et al.*, 2009; *Abdu et al.*, 2009b and references therein]. The coupling of the ionospheric plasma dynamics and

91 neutral atmosphere wave dynamics has been extensively studied in the last 30 years.
92 However, it seems that a conclusive scenario for explaining the ionosphere-atmosphere
93 coupling dynamics, as related to spread F development, has not yet been developed. To
94 date, the nature of the perturbation is widely believed to be gravity waves. These waves
95 are normally generated through the process of vertical movement of air-parcels forced
96 by convections, front activity and topography in the troposphere. These waves can
97 propagate above 100 km, even up to 200 km in the ionosphere [*Takahashi et al.*, 2009].
98
99 In the following sections of this work, we describe an experimental method for the
100 calculation of the initial amplitude of perturbation that can be useful for application in
101 numerical simulation of bubbles. The ionograms analyzed correspond to the station of
102 Cachimbo.
103
104 **2. Initial amplitude**
105 The works of *Ossakow et al.* [1979], *Ossakow* [1981], *Zalesak and Ossakow* [1980],
106 *Zalesak* [1979] demonstrated/confirmed that a small perturbation at the base of the
107 equatorial F region at post sunset hours leads to the formation of irregular structures.
108 When a perturbation is present (e.g. sinusoidal) along the zonal direction (east-west) a
109 polarization electric field is established and then the less dense (depletion) plasma
110 moves upward. In *Ossakow et al.* [1979], the initial perturbation is defined by an
111 analytic function in the form
112
113 $$N(x,z,0) = N_0(z)\left[1 - A\cos\left(\frac{2\pi}{\lambda}x\right)\right] \quad (1)$$
114

where N is the plasma density, N_0 is the background initial plasma density or equilibrium density, A is the amplitude of the initial perturbation and λ is the wavelength of the perturbation. Equation (1) represents a mesh in height (z) and horizontal (East-West) direction (x) with a maximum depression surrounding x=0. Many authors use a fixed value (5% or 0.05 in decimal) for the amplitude A in their numerical simulation of bubbles [see, for example, *Ossakow et al.*, 1979; *Huang and Kelley*, 1996a; *Sekar et al.,* 2001]. Although those authors use always a fixed value for the perturbation, it is clear that A should vary from one day to the other, because the ionospheric conditions vary on a day to day basis. Additionally, A depends strongly on the source that originates the perturbation (for example gravity waves). According to *Mendillo et al*. [1992] and *Sekar et al.* [1995] there is a significant number of observed onset conditions for the post-sunset equatorial spread F that are not evidently associated with the required (5%) seed perturbation as assumed in earlier simulation studies. Using a simulation model, *Sekar et al.* [1995] have shown that the threshold perturbation can be as low as 0.5% (or 0.005 in decimal) for the plasma bubble development. This result suggests possible values of initial amplitude smaller than 5%. The simulation works developed until now do not provide a method to calculate the parameter A.

In this work we propose an experimental method to calculate the value of parameter A from ionograms that better represent the conditions of the event to simulate. This method is described in the following session.

3. Experimental method

139 The initial amplitude of the perturbation can be defined as the fractional change of the
140 electron number density $\delta N/N$ [e.g. *Kherani*, 2002; *Sekar and Kherani*, 2002]. At the
141 equatorial *F* region, under the RTI mechanism, this change ($\delta N/N$) is produced by the
142 combination of vertical ($\vec{E}x\vec{B}/B^2$) drift and the growth of the instability. Considering a
143 limited region in space, a positive vertical drift lifts up a portion of the layer base
144 introducing variations in its density and height in such a way that when part of the layer
145 base is elevated in height this is seen as a decrease in density at the same region. In the
146 works describing numerical simulation of bubbles, this density change can be seen by
147 the vertical rise of an isodensity contour from the base of the layer. The initial top
148 height of the isodensity curve depends on the initial perturbation generated by the
149 polarization field. In other words, the amplitude of the initial plasma density
150 perturbation is an essential parameter for growth of the plasma instability under
151 favorable conditions.
152
153 In some cases the base of the main trace (F) in ionograms can show a diffuse region.
154 This diffuse echo (patch) has been interpreted as the signature of plasma instability.
155 Thus the evolution of the instability can be tracked by following the movement of the
156 irregularity at the base of the F layer trace from consecutive ionograms. Figure 1a
157 shows a sequence of ionograms obtained in the station of Cachimbo on December 3,
158 2002 during the COPEX campaign. We can observe the diffuse echoes (patches) in the
159 bottomside F trace and their displacement in frequency and height from one ionogram
160 to the other. The accuracy with which height and frequency of the diffuse echo on main
161 trace can be measured depends on the reading accuracy used in reducing the ionograms.
162 In this work the convention adopted for reading the upper frequency limit of the diffuse
163 echo is that it should be contiguous to the $h'(f)$ trace (see the vertical arrows in Fig.

164 1a). The upper limit of the echo corresponds to the top height of the isodensity curve in
165 Figure 1b, according to the following reasoning: as the irregularity (bubble) evolves it
166 grows in height inside the F layer (the top of the isodensity curve reaches distinct
167 heights at different times). In the ionograms this movement is seen as a bi-dimensional
168 (height and frequency) evolution of the top of the irregularity (bubble) over the
169 ionogram main trace, which means equivalence between the position in space and time
170 of the top of the irregularity and the isodensity curve top. In this way, after a time lag t,
171 the new vertical position of the top of an isodensity curve will be detected in the
172 ionogram as a frequency variation as the top of the irregularity evolves above the main
173 trace. Under this assumption, once the frequency evolution is known, we can obtain the
174 new height of the irregularity over the trace. The Digisonde precision for measuring
175 virtual height is ±5 km but the Sao-Explorer program [*Galkin et al.,* 2008] can
176 interpolate values with 0.1 km of precision. However, we must be careful not to confuse
177 precision and observational error in the virtual height.
178
179 For the sequence of ionograms in Fig. 1 the values obtained for height and frequency at
180 the upper end of the patch, marked by horizontal and vertical arrows, respectively, in
181 the ionograms, are (t_0=22:40 UT, no diffuse echo, only satellite trace seem as precursor
182 of the instability), (t_1=22:45 UT, h_1=380.6 km, f_1=2.0 MHz), (t_2=22:50 UT,
183 h_2=399.2 km, f_2=2.2 MHz), (t_3=22:55 UT, h_3=413.6 km, f_3=2.4 MHz). The
184 frequencies f_i are obtained at the upper limit of the diffuse echo in each ionogram and
185 the heights h_i correspond to the virtual height at the frequency f_i ($h_i = h'(f_i)$). In the
186 context of the plasma depletion in the bottomside F-layer, the irregularities or structures
187 can be seen as isodensity contour in evolution, where the plasma decrease rate is

188 associated with the rate of change in height of the isodensity contour (Figures 1a and
189 1b). In Figure 1b the sequence of isodensity curves represents the height evolution of
190 the irregularity seen in part (a) of the figure. The heights marked with arrows
191 correspond to the height at the limit of frequency of a diffuse echo on the main profile
192 of density (ionogram). In Figure 1c the sequence of profiles represents a schematic of
193 the time evolution of the vertical electron density profiles as the irregularity develops.
194 To determine the initial amplitude *A* we assume a linear development of the irregularity
195 during its initial phase in such a way that the fractional change of the electron number
196 density, *δN/N*, can be calculated from the rate of change (or fractional variation) in
197 virtual height of two consecutive positions of upper limit of the diffuse echo, that is
198 $\delta N / N \approx \Delta h / h$. Thus the initial amplitude can be calculated from the
199 expression $A \approx h_2 / h_1 - 1$. As an example of the method, using the data from Figure 1a,
200 h_1=380.6 km, h_2=399.2 km we obtain $A = 0.048$ and the vertical velocity of the
201 irregularity $(h_3 - h_1)/2\Delta t = 55 m/s$. This velocity is the result of the action of two
202 electric fields: the ambient electric field (E_0) and the electric field of the perturbation
203 (E_1). The perturbation electric field (E_1) is not easy to measure directly at the moment
204 that the irregularity arises. In a first approach, E_1 can be obtained from the numerical
205 solution of the differential equation for the perturbation electrical potential (Φ_1). On the
206 other hand, in the differential equation the source term depends on the ambient electric
207 field and on the collision frequency in the form $1/\nu_i$. These two parameters can
208 influence the numerical solution of the electrical potential. Additionally, the
209 perturbation in the density evolves according to the RTI growth rate, γ [for more
210 details see, for example, *Huang and Kelley*, 1996a].
211

From the technical point of view our observations were limited to the presence of irregularities visible in the ionograms at frequencies larger than 1.5 MHz. During the night the F trace is visible from 1.5 MHz onwards (on average). Under these conditions, if irregularities are present at frequencies less than 1.5 MHz they can not be detected with the technique of vertical sounding. We have applied the described method to 10 days of data obtained at the equatorial station Cachimbo during the COPEX campaign.

4. Results and discussion

The results of the experimental method used to calculate the amplitude A of the initial perturbation are shown in Table 1 for different events observed in Cachimbo, together with other relevant parameters such as the spread-F onset time (TimeI) and the time of occurrence of the maximum in the vertical drift pre-reversal enhancement (TimeP), the Dst index and the solar flux at 10.7 cm (F10.7). The values obtained for the initial amplitude (A) vary between approximately 0.03 and 0.08. The irregularity onset time (TimeI) varies between 22:10 and 23:15 UT. Comparing TimeI and TimeP, it is possible to conclude that the irregularities initiate only after the vertical drift, V_0, reaches its maximum value (Vp), as already reported by *Nelson et al.* [1986]. In Figure 2 we plot the amplitude versus the perturbation electric field. The perturbation electric field was calculated based on the assumption that the total electric (E) responsible for the bubble rise is equal to the sum of the ambient electric field (E_0) and the perturbation electric field (E_1). Around sunset the ambient electric field can be calculated from the vertical drift according to the expression $\Delta h'F / \Delta t \approx E_0 / B$ [*Bittencourt and Abdu*, 1981; *Batista et al.*, 1986], where *h'F* is the minimum virtual height of the *F* layer, *t* is time and *B* is the geomagnetic field. Similarly the total electric field (E) responsible for the bubble rise can be obtained from the expression $\Delta h_C / \Delta t \approx E / B$, where

237 $\Delta h_C = h'(f_j) - h'(f_i)$. In Figure 2 even with so few points we can observe a definite
238 dependency of the behavior of the amplitude with the perturbation field (E_1). The two
239 curves plotted in the graphic represent linear and power fitting to the data. This result
240 represents an effort to obtain the initial amplitude and the perturbation electric field at
241 the beginning of the irregularities. According to our results, it seems that there is a
242 threshold (approximately equal to 0.03) in the relative amplitude above which
243 irregularities/bubbles can be generated in the equatorial ionospheric region under study.
244 This threshold is lower than that used by some author in theoretical simulation of
245 plasma bubbles, but is not as low as that found in the work of *Sekar et al*. [1995], that
246 found a threshold of 0.005. As we have used an experimental methodology to determine
247 the threshold, it is possible that time and/or height resolution of our data introduce
248 limitations in determining thresholds lower than 0.03. Another possibility for the higher
249 threshold found in the present work as compared to *Sekar et al*. [1995] is the dataset
250 used in the present study, that does not show the very high upward drift velocity needed
251 for the plasma bubble development with the low threshold found by *Sekar et al*. [1995].
252 The verification/validation of those hypothesis can be clarified with the aid of a
253 numerical simulation code of bubbles in which all the atmospheric/ionospheric
254 parameters are known (vertical profile of plasma, neutral temperature, electric field,
255 collision frequency, etc), and the amplitude varies from one simulation to the other. We
256 do not try to infer the nature of the seed perturbation in the present study but only to
257 show the effect of the initial amplitude and its correlation with other atmospheric
258 parameters. The combination of the parameters, A, E_1, ν_i (collision frequency) can play
259 an important role in the determination of the onset time of occurrence of the
260 irregularities.
261

Figure 3 shows the temporal variation of the vertical drift for three events. In order to facilitate the analysis of this figure, we will compare first events on 16 and 29 of November. In this figure we can observe that the peak of the vertical velocity, Vp is higher in the event of day 16 (56 m/s) than in the November 29 event (46 m/s) but the irregularity starts earlier in the event of day 29 (see Table 1). For this discussion we will need the expression for the linear growth rate (horizontal mode of propagation and without neutral wind) which is given by [*Huang and Kelley*, 1996a]

$$\gamma = \frac{1}{N_0}\frac{\partial N_0}{\partial z}\left(\frac{g}{\nu_i} + \frac{E_0}{B}\right) - \beta \qquad (2)$$

where g is the acceleration due to gravity, ν_i is the collision frequency and β is the recombination coefficient. Based on this equation, γ increases when ν_i decreases. The minimum F layer virtual heights at the time of the perturbation onset in the ionogram were, respectively, 423 and 342 km on the 16 and 29 November, but between 2100 and 2200 UT the heights were very similar on both days. According to various simulation works the instability begins to grow 20 to 30 minutes after the perturbation in the bottomside starts. This time lag that the phenomenon takes to evolve and to be observed in the ionograms is an important point to be considered. In Figure 3 we can observe that the drift velocity between 21:00 and 22:00 UT is very similar in the events on 16 and 29 November. Under these circumstances the bottomside F layer vertical rise was similar in the two days. This can suggest that, for these particular events, the ambient electric field, E_0, does not fully control the evolution of the instability. Nonetheless its contribution is important in the development of the structures, when the perturbation occurs in the bottomside. In Table 1 we can see that the solar flux was larger in the event of November 16 as compared to November 29. The increase of neutral temperature with the solar flux can increase the collisions between neutral particles with

286 ions [see for example, *Schunk and Nagy*, 2009] contributing to the decrease of g/ν_i on
287 16 Nov as compared with 29 Nov. This could decrease the instability growth rate and
288 hence cause a delay in the time of occurrence of the irregularities. Under these
289 conditions the 29 Nov event should evolve faster compared to the 16 Nov event, as
290 indeed observed. On the other hand, at the time of the irregularity onset, the layer is
291 higher on the 16th than on the 29th, which could compensate the increase in collision
292 frequency due to temperature increase on 16th. Additionally, it is important to
293 emphasize that γ represents a measurement of the evolution of the instability when the
294 initial density perturbation occurs. The difference of initial amplitude between the
295 events can also play an important role in the development of the instability. As noted
296 from Table 1, the amplitude A is twice larger on 29th as compared to the 16th, suggesting
297 that initial density perturbation is larger on 29th. *Abdu et al.* [2009] and *Kherani et al.*
298 [2009] have shown that for similar electric field strength as here (56 and 46 m/s on 16th
299 and 29th, respectively), the bubble growth is larger when the initial amplitude is large.
300 On this basis it is expected that on 29th bubble will grow faster. In this context, the
301 results presented here are the first to directly estimate the parameter *A* based on
302 ionograms and relate it with the bubble growth on two nights.
303
304 Figure 4 shows a plot of the variation of delay (the difference between TimeI and
305 TimeP) with the perturbation amplitude. In the figure we can see that the delay
306 decreases with the increase of the amplitude (a linear and exponential fit to the data
307 points are also shown in the figure). This interesting result suggests a straight
308 relationship between the hour of occurrence of the irregularity and the amplitude of the
309 initial perturbation in density, *A*.
310

311 The event that showed the largest delay (~1 hour) occurred on October 27. This large
312 delay between the peak of the vertical velocity and the beginning of the irregularity can
313 be attributed to a low value of E_0 or V_0 (surrounding the maximum) probably caused
314 by a magnetic disturbance (Dst= -61). The initial amplitude for the 27 Oct event was
315 very similar to the event on 16 Nov (~0.03) but the delay was ~30 min larger in the first
316 event as compared to the second. In order to support the theory about the effect of the
317 electric field, E_0 and collision frequency, we analyzed the event of 14 Oct (not included
318 in Table 1). For the 14 Oct event (Dst= -60, F10.7= 180) the maximum pre-reversal
319 vertical drift was Vp = 23 m/s at 22:10 UT and did not present/display irregularities.
320 Comparing the events of 14 and 27 Oct it is evident that the low value of the vertical
321 drift (23 m/s) affected the development of the instability. According to *Huang and*
322 *Kelley* [1996b], the equatorial electric fields associated with magnetic storms cannot
323 produce plasma bubbles when the F layer is low. This is because the growth rate of the
324 Rayleigh-Taylor instability is low for low F layer height. In comparison with the
325 previous explanation, *Woodman* [1994] argued that the plasma bubbles could be seeded
326 by the prereversal enhancement of the east-west electric field.
327
328 **5. Conclusions**
329 The main purpose of this work was the development of an experimental method for the
330 calculation of the initial amplitude of perturbation. Our results showed a variation
331 between 0.03 and 0.08 for the fractional change in the number density in the bottomside
332 of the F-region. A threshold of 0.03 was found for the initial amplitude of perturbation,
333 necessary for the development of irregularities in the equatorial ionospheric region
334 under study. It is possible that lower threshold values, compatible with the results by
335 *Sekar et al*. [1995] could be attained if the methodology was applied to distinct data sets

with different time and height resolution. An important result was the linear relationship between the hour of occurrence (or delay) of the irregularity and the initial amplitude showing that the delay tends to decrease with the increase of the initial amplitude. The results presented here are the first to directly estimate the parameter *A* based on ionograms and relate it with the bubble growth on two nights. Motivated by the obtained results, the experimental method will be applied to other ionospheric stations over the magnetic equator and will be used in numerical simulation with the intention to simulate the time of occurrence of the bubbles experimentally detected.

Acknowledgements. The authors wish to acknowledge the support from FAPESP through the process 2010/05698-8 through which the visit of Dr. Carrasco to the Aeronomy Division, DAE/INPE was made possible. The authors thank the referees for their useful comments.

References

Abdu, M. A., I. S. Batista, and J. A. Bittencout (1981), Some characteristics of equatorial spread F at the magnetic equatorial station Fortaleza, *J. Geophys. Res*., 86, A8, 6836-6842.

Abdu, M. A., I. S. Batista, B. W. Reinisch, J. R. de Souza, J. H. A. Sobral, T. R. Pedersen, A. F. Medeiros, N. J. Schuch, E. R. de Paula, and K. M. Groves (2009a), Conjugate Point Equatorial Experiment (COPEX) campaign in Brazil: Electrodynamics highlights on spread F development conditions and day-to-day variability, *J. Geophys. Res*., 114, A04308, doi:10.1029/2008JA013749.

Abdu, M. A., E. A. Kherani, I. S. Batista, E. R. Paula, D. C. Fritts, and J. H. A. Sobral

(2009b), Gravity wave initiation of equatorial spread F /Plasma bubble irregularities based on observational data from the SpreadFEx campaign, *Ann. Geophys.*, *27*, 2607-2622.

Batista, I. S., M. A. Abdu, J. A. Bittencourt (1986), Equatorial F region vertical plasma drifts: Seasonal and longitudinal asymmetries in the American sector, *J. Geophys. Res.*, *91*, 12,055-12,064.

Batista, I. S., M. A. Abdu, A. J. Carrasco, B. W. Reinisch, E. R. Paula, N. J. Schuch, and F. Bertoni (2008), Equatorial spread F and sporadic E-layer connections during the Brazilian Conjugate Point equatorial Experiment (COPEX), *J. Atmos. Sol. Terr. Phys.*, *70*, 1133-1143, doi:10.1016/j.jastp.2008.01.007.

Bittencourt, J. A., and M. A. Abdu (1981), A Theoretical comparison between apparent and real vertical ionization drift velocities in the equatorial F region, *J. Geophys. Res.*, *86,* A4, 2451-2454.

Booker, H. G., and H. W. Wells (1938), Scattering of radio waves in the F-region of the ionosphere, *Terr. Magn. Atmos. Electr.*, *43*, 249-256.

Fejer, B. G., L. Scherliess, and E. R. Paula (1999), Effects of the vertical plasma drift velocity on the generation and evolution of equatorial spread F, *J. Geophys. Res.*, *104,* A9, 19859-19869.

Fritts, D. C., M. A. Abdu, I. S. Batista, P. P. Batista, R. Buriti, B. R. Clemesha, T. Dautermann, E. R. de Paula, J. Fechine, B. G. Fejer, D. Gobbi, J. Haase, F. Kamalabadi, E. A. Kherani, B. Laughman, P. P. Lima, H.-L. Liu, A. Medeiros, P.-D. Pautet, D. M. Riggin, F. S. Rodrigues, F. São Sabbas, J. H. A. Sobral, P. Stamus, H. Takahashi, M. J. Taylor, S. L. Vadas, F. Vargas, and C. M. Wrasse (2009), Overview and summary of the Spread F Experiment (SpreadFEx), *Ann. Geophys., 27*, 2141–2155.

385 Galkin, I. A., G. M. Khmyrov, B. W. Reinisch, and J. McElroy (2008), The SAOXML 5:
386 New format for ionogram-derived data, in *Radio Sounding and Plasma Physics, AIP*
387 *Conf. Proc. 974*, 160-166.

388 Huang, C. S., and M. C. Kelley (1996a), Nonlinear evolution of equatorial spread F:
389 Gravity wave seeding of Rayleigh-Taylor instability, *J. Geophys. Res*., *101,* A1, 293-
390 302.

391 Huang, C. S., and M. C. Kelley (1996b), Nonlinear evolution of equatorial spread F.
392 Plasma bubbles generated by structured electric fields, *J. Geophys. Res*., *101,* A1, 303-
393 313.

394 Kherani, E. A., Investigations of F region plasma instabilities under different
395 background conditions, Ph.D. thesis, 92 pp., Mohanlal Sukhadia Univ., Udaipur, India,
396 2002.

397 Kherani, E. A., M. A. Abdu, E. R. de Paula, D. C. Fritts, J. H. A. Sobral, and F. C. de
398 Meneses Jr. (2009), *Ann*. *Geophys*., *27*, 1657-1668.

399 Lyon, A. J., N. J. Skinner, and R. W. Wright (1961), Equatorial spread F at Ibadan,
400 Nigeria, *J. Atmos. Terr. Phys*., 21, 100.

401 Mendillo, M., J. Baumgardner, X, Pi, P.J., Sultan, and R. T. Tsunoda (1992), Onset
402 conditions for equatorial spread F, *J. Geophys. Res*., *97*, doi:10.1029/92JA00647,
403 13865-138761.

404 McNamara, L. F., J. M. Retterer, M.A. Abdu, I. S. Batista, B. W. Reinisch (2008), F2
405 Peak parameters, drifts and spread F derived from digisonde ionograms for the COPEX
406 campaign in Brazil, *J. Atmos. Solar-Terr. Phys. 70.* 1144–1158.

407 Nelson, O. R., M. A. Abdu, and I. S. Batista (1986), Equatorial F-region irregularity
408 latitudinal extension and dynamo electric field, *J. Atmos. Terr. Phys*., *48*, 2, 181.

409 Ossakow, S. L. (1981), Spread F theories-a review, *J. Atmos. Terr. Phys*., *43*, 5/6, 437-
410 452.

411 Ossakow, S. L., S. T. Zalesak, and B. E. McDonald (1979), Nonlinear Equatorial Spread
412 F: Dependence on Altitude of the F Peak and Bottomside Background Electron Density
413 Gradient Scale Length, *J. Geophys. Res*., *84*, A1, 17-29.

414 Reinisch, B. W., M. Abdu, I. Batista, G. S. Sales, G. Khmyrov, T. A. Bullett, J. Chau, and
415 V. Rios (2004), Multistation digisonde observations of equatorial spread F in South
416 America, *Ann. Geophys. 22*, 3145–3153.

417 Schunk, R., and A. Nagy (2009), *Ionosphere Physics, Plasma Physics, and Chemistry*,
418 Cambridge.

419 Sekar, R., and E. A. Kherani (2002), Effects of molecular ions on the collisional
420 Rayleigh-Taylor instability: Nonlinear evolution, *J. Geophys. Res*., *107*, A7, 1139-1147,
421 doi: 10.1029/2001JA000167.

422 Sekar, R., E. A. Kherani, P. B. Rao, and A. K. Patra (2001), Interaction of two long-
423 wavelength modes in the nonlinear numerical simulation model of equatorial spread F,
424 *J. Geophys. Res*., *106*, A11, 24,765-24,775.

425 Sekar, R., R. Suhasini, and R. Raghavarao (1995), Evolution of plasma bubbles in the
426 equatorial F region with different seeding conditions, *Geophys. Res. Lett*., *22*, 885-888.
427 Takahashi, H., M. J. Taylor, P.-D. Pautet, A. F. Medeiros, D. Gobbi, C. M. Wrasse, J.
428 Fechine, M. A. Abdu, I. S. Batista, E. Paula, J. H. A. Sobral, D. Arruda, S. L. Vadas,
429 F. S. Sabbas, and D. C. Fritts (2009), Simultaneous observation of ionospheric plasma
430 bubbles and mesospheric gravity waves during the SpreadFEx Campaign, *Ann.*
431 *Geophys.*, *27*, 1477-1487.

432 Tsunoda, R. T. (2008), Satellite traces: An ionogram signature for large-scale wave

433 structure and a precursor for equatorial spread F, *Geophys. Res. Lett*., 35, L20110,
434 doi:10.1029/ 2008GL035706.

435 Woodman, R. F. (1994), Equatorial ionospheric irregularities as observed by the
436 Jicamarca radar, in Low-Latitude Ionospheric Physic**s**, F. S. Kuo, Pergamon, New York.

437 Zalesak, S. T. (1979), Fully Multidimensional Flux-Corrected Transport Algorithms for
438 Fluids, *J. Comput. Phys*., *31*, 335-362.

439 Zalesak, S. T., and S. L. Ossakow (1980), Nonlinear Equatorial Spread F: Spatially
440 Large Bubbles Resulting From Large Horizontal Scale Initial Perturbations, *J. Geophys.*
441 *Res*., *85*, A5, 2131-2142.

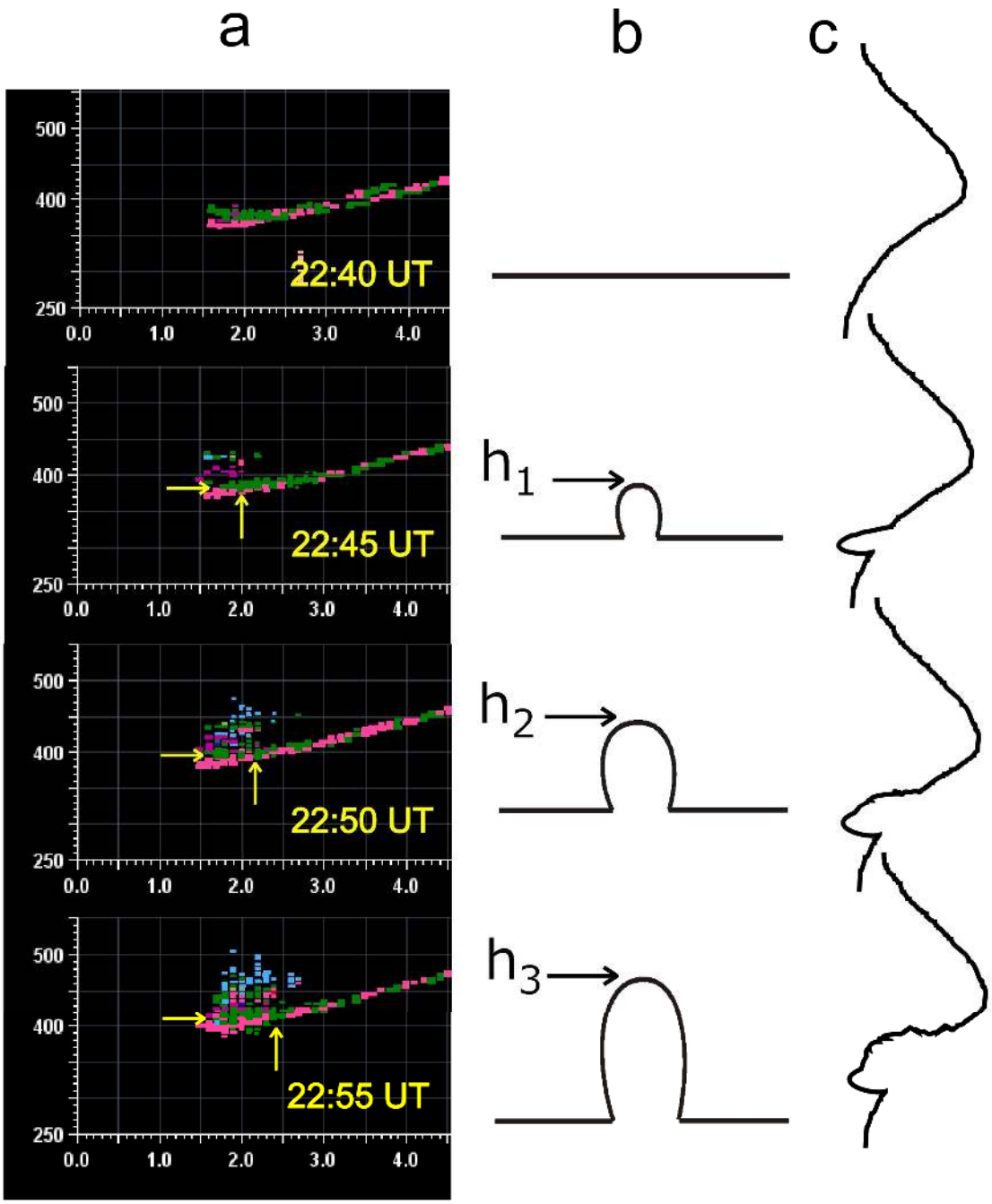

Fig. 1 Illustrative description of the experimental method applied to the ionograms for December 3, 2002 from 22:40 to 22: 55 UT. In part (a) of the figure we can see, from the ionograms, the growth of the irregularity at the base of F layer. Part (b) illustrates the isodensity contour corresponding to each ionogram. Part (c) shows a schematic illustration of the electron density vertical profile.

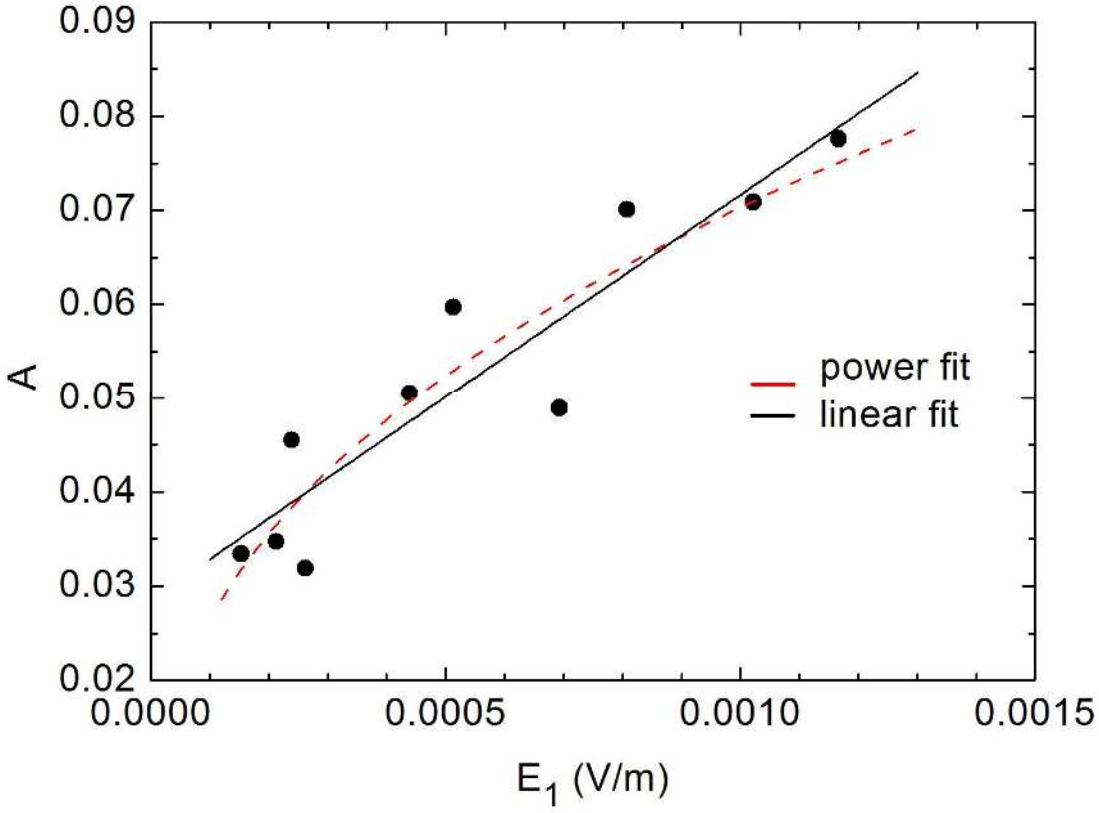

449

450 **Fig. 2** Variation of the amplitude with the perturbation electric field. Two functions

451 were fit to the data.

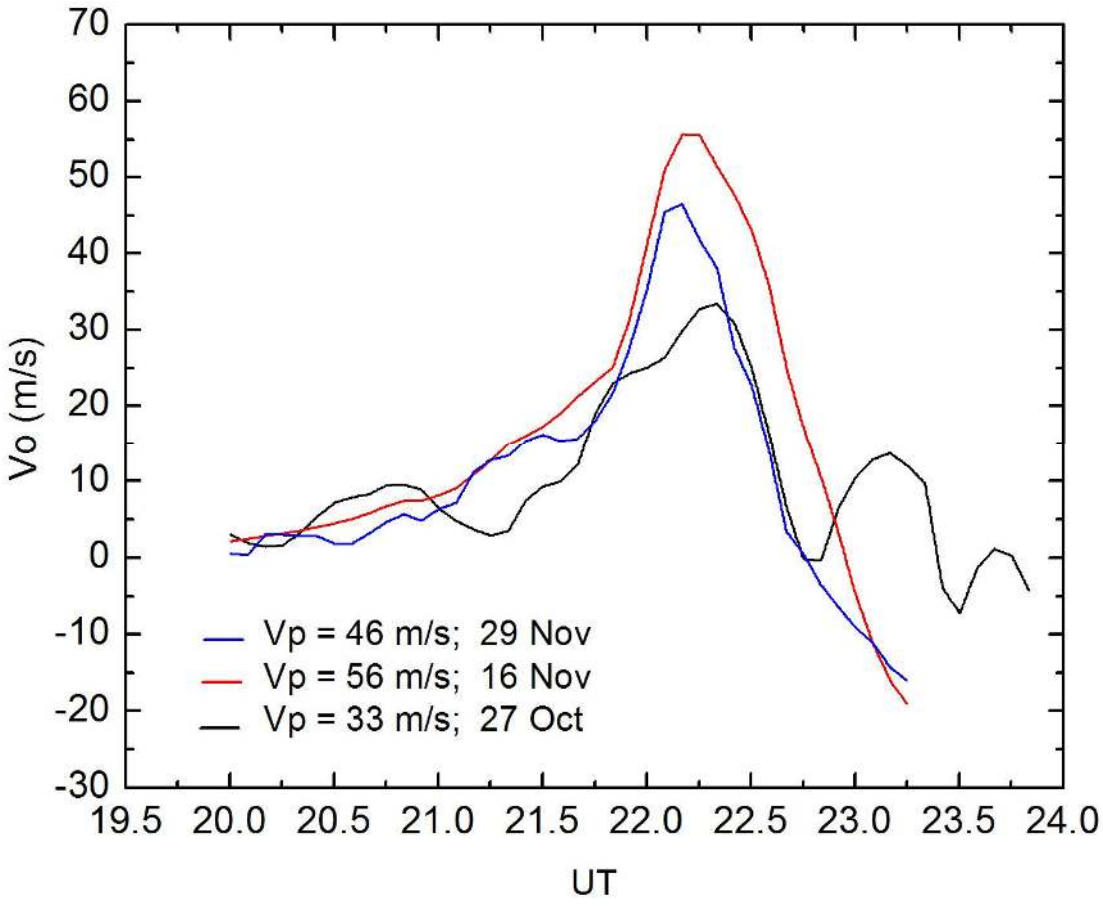

452

453 **Fig. 3** Variation of the vertical plasma drift as a function of the hour (UT) for three

454 days over Cachimbo from data collected during the COPEX campaign.

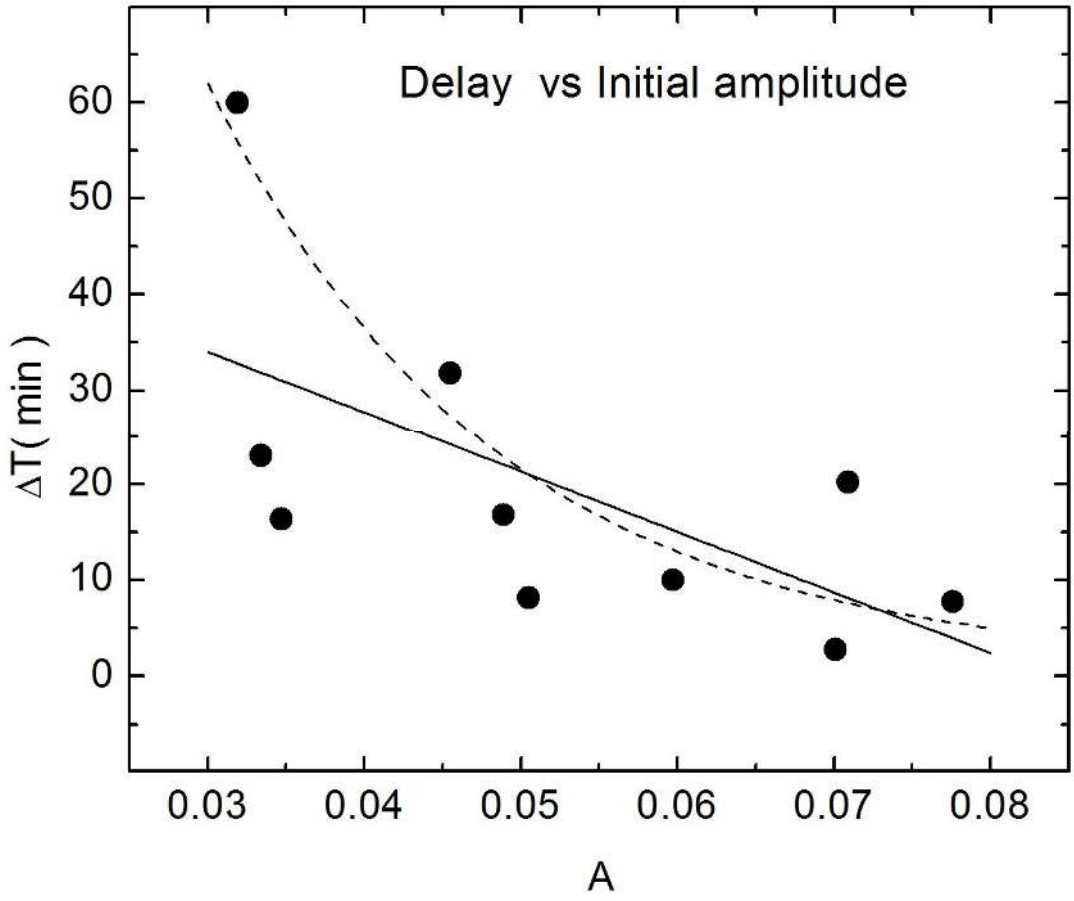

455

456 **Fig. 4** Variation of the delay with the initial amplitude of perturbation. Two functions

457 were fit to the points. The delay decreases as the amplitude increases.

Table 1
List of the events used in the study

Event	TimeI (UT)	TimeP (UT)	Dst	F10.7	A
6 Oct 2002	**22:30**	**21:58**	**-60**	**161.7**	**0.0455**
8 Oct 2002	**22:25**	**22:05**	**-53**	**165.4**	**0.0709**
11 Oct 2002	**22:05**	**21:49**	**-35**	**179.4**	**0.0347**
22 Oct 2002	**22:10**	**22:02**	**-19**	**173.3**	**0.0505**
27 Oct 2002	**23:15**	**22:15**	**-61**	**157.1**	**0.0319**
6 Nov 2002	**22:25**	**22:15**	**-51**	**184.5**	**0.0597**
13 Nov 2002	**22:15**	**22:07**	**-31**	**167.1**	**0.0776**
16 Nov 2002	**22:30**	**22:07**	**-28**	**196.1**	**0.0334**
29 Nov 2002	**22:10**	**22:07**	**-23**	**143.0**	**0.0701**
3 Dec 2002	**22:45**	**22:28**	**-21**	**148.3**	**0.0489**